







Interplay of broken symmetry and delocalized excitations in the insulating state of 1T-TaS₂

Xun Jia ^{1,*}, Anubhab Haldar ², Jungho Kim,³ Yilin Wang,⁴ Gilberto Fabbris,³ Karl Ludwig,^{5,6} Stefanos Kourtis,⁷ Mary Upton,³ Yu Liu ⁸, Wenjian Lu,⁸ Xuan Luo ⁸, Yu-Ping Sun ^{8,9,10}, Diego Casa,³ Sahar Sharifzadeh,^{2,5,6,†} Pierre T. Darancet,^{11,‡} and Yue Cao ^{1,12,§}

¹Materials Science Division, Argonne National Laboratory, Lemont, Illinois 60439, USA

²Department of Electrical and Computer Engineering, Boston University, Boston, Massachusetts, USA

³Advanced Photon Source, Argonne National Laboratory, Lemont, Illinois 60439, USA

⁴School of Future Technology, University of Science and Technology of China, Hefei, Anhui 230026, China

⁵Department of Physics, Boston University, Boston, Massachusetts 02215, USA

⁶Division of Materials Science and Engineering, Boston University, Boston, Massachusetts, USA

⁷Institut quantique & Departement de physique, Universite de Sherbrooke, Quebec J1K 2R1, Canada

⁸Key Laboratory of Materials Physics, Institute of Solid State Physics, HFIPS, Chinese Academy of Sciences, Hefei 230031, China

⁹High Magnetic Laboratory, HFIPS, Chinese Academy of Sciences, Hefei 230031, China

¹⁰Collaborative Innovation Centre of Advanced Microstructures, Nanjing University, Nanjing 210093, China

¹¹Center for Nanoscale Materials, Argonne National Laboratory, Lemont, Illinois 60439, USA

¹²Pritzker School of Molecular Engineering, University of Chicago, Chicago, Illinois 60637, USA



(Received 5 October 2022; revised 31 July 2023; accepted 10 October 2023; published 2 November 2023)

Coexistence of localized and extended excitations is central to the macroscopic properties of correlated materials. For *5d* transition-metal compounds, electron correlations alone generally do not lead to a metal-insulator (Mott) transition, with insulating behavior usually resulting from their coupling with magnetic ordering and/or structural distortions. 1T-TaS₂ is a prototypical example of such correlated insulating behavior, with a high-symmetry metallic phase transforming into a distorted, charge-density wave (CDW) insulating state at low temperatures. The nature of the insulating phase as well as the existence and relevance of the localized electron physics remains debated. We resolve this standing controversy in 1T-TaS₂ combining resonant inelastic x-ray spectroscopy and first-principles calculations. We observe five electronic excitations arising from the interband transitions of the Ta *5d* orbitals and the S *3p* ligand state, with none of the excitations on the order of the Mott gap. These excitations cannot be explained within the framework of standard multiplet calculations that assume a localized wave function, but instead, are captured by a band-theory framework accounting for the low symmetry of the crystal field in the CDW state. Our findings suggest that the electronic properties of 1T-TaS₂ are dominated in the visible by both plasmonic quasiparticles and interband transitions, with no resonance associated with a putative Mott transition observed in the 0–3 eV energy range. Our discovery provides insights into the electron localization and the Mott vs band-insulator debate in 1T-TaS₂ and other transition-metal materials.

DOI: [10.1103/PhysRevB.108.205105](https://doi.org/10.1103/PhysRevB.108.205105)

I. INTRODUCTION

Metal-insulator “Mott” transitions [1] canonically involve localized electronic states, such as electrons in *d* and *f* orbitals with low principal quantum numbers, leading to repulsive Coulomb interactions outcompeting the delocalization from the orbital overlap. Mott insulators are ubiquitous in *3d* transition-metal compounds, with the most notable example being the cuprates at the center of high-*T_C* superconductor research for the last few decades [2]. In contrast, when the or-

bitual wave functions of the constituting atoms becomes more extended, e.g., in most *5d* transition-metal compounds, electronic correlations alone generally cannot lead to localization; and metal-insulator transitions usually involve additional energy scales, such as polaronic effects and spin-orbit coupling. These additional energy scales naturally raise the question of the transferability of the phenomenological models developed to describe *3d* transition-metal compounds to their heavier counterparts. In recent years, studies of the iridates [3–6] and lacunar spinel GaTa₄Se₈ [7] have shown that the combination of spin-orbit coupling and Coulomb repulsion can lead to the Mott insulating behavior. In contrast, the nature of the excitations in *5d* insulators involving charge-density waves (CDW) is less understood and raises the question on the transferability of the models derived from intrinsically localized electronic states.

Tantalum disulfide (1T-TaS₂) is a layered *5d* transition compound among the larger family of transition-metal

*Present address: Multi-disciplinary Research Division, Institute of High Energy Physics, Chinese Academy of Sciences, Beijing 100049, People’s Republic of China; jiaxun@ihep.ac.cn

†ssharifz@bu.edu

‡pdarancet@anl.gov

§yue.cao@anl.gov

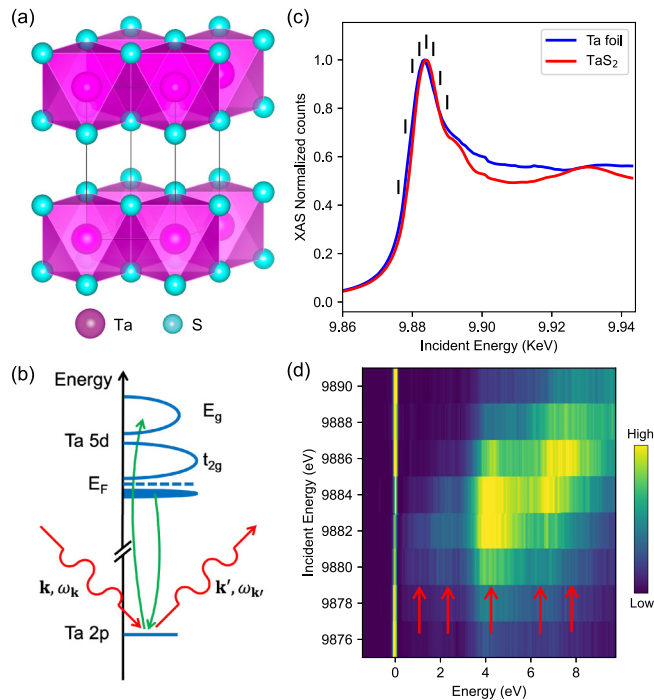


FIG. 1. Energy-loss spectra of $1T$ -TaS₂ across Ta L_3 resonance. (a) Crystal structure of $1T$ -TaS₂. Each Ta atom is at center of Ta-S octahedron. (b) Schematics of RIXS process at Ta L_3 edge. (c) X-ray absorption spectra at Ta L_3 edge for $1T$ -TaS₂ and reference Ta foil, respectively. Incident energies for RIXS measurements in panel (d) are marked using black vertical lines. (d) RIXS spectra as function of incident energy across Ta L_3 resonance at 10 K. Red arrows are used as guide to eyes to mark energy-loss features.

dichalcogenides with charge orders that are actively studied due to their proximity to superconductivity and potential applications in quasi-two-dimensional electronics [8,9]. In Fig. 1(a), we show the crystal structure of $1T$ -TaS₂ in the high-symmetry metallic phase. The crystal is centrosymmetric with the Ta atom sitting at the center of a tilted sulfur (S) octahedron. $1T$ -TaS₂ has a commensurate, “star-of-David”-type CDW $Q_{\text{CCDW}} = (3/13, 1/13, 1/3)$ below 225 K, a nearly commensurate CDW (NCDW) at $Q_{\text{NCDW}} = (0.245, 0.068, 1/3)$ below 355 K, and an incommensurate CDW of $Q_{\text{ICDW}} = (0.283, 0, 1/3)$ above 355 K [9,10]. The symmetry-broken phases are significantly less conductive than their high-symmetry counterpart, and the transition from the NCDW into the commensurate CDW (CCDW) phase features a tenfold increase in resistivity [9].

Despite decades of research, the nature of the insulating state in the CCDW phase $1T$ -TaS₂ is actively debated. On the one hand, the 13 Ta atoms per CCDW supercell have a nominal $5d^1$ electronic configuration [9,11,12], prompting the widely accepted argument that the Coulomb repulsion plays a vital role and that the onset of insulator behavior is of Mott type. On the other hand, the band dispersion in the CCDW phase observed using the angle-resolved photoemission spectroscopy can be captured reasonably well through band folding without significant electron correlation. In this latter scheme, the band gap can be induced, e.g., through other mechanisms such as dimerization, suggesting an in-plane

band insulator with a one-dimensional out-of-plane metallic order subsequently broken by a Peierls-type or Anderson-like localization [13]. These competing pictures have been actively debated over the last few years [13–17] with their fundamental difference in whether the electron wave function is localized or extended. Recently, $1T$ -TaS₂ was proposed as a possible quantum spin liquid (QSL) [18] partially supported by specific-heat and muon spin-resonance studies [19,20]. The QSL proposal was closely linked to the Mott picture, further highlighting the need to understand the nature of the electron wave functions in $1T$ -TaS₂.

In this paper, we study the electronic excitations in $1T$ -TaS₂ combining resonant inelastic x-ray scattering (RIXS) and theoretical simulations. For $3d$ transition-metal compounds, excitations from local electronic interactions can be measured with RIXS and calculated using orbital multiplets [21]. On the RIXS spectra, a local excitation exists corresponding to the Mott gap of the respective material. Moreover, the qualitative and quantitative agreements between RIXS measurements and orbital multiplet calculations have been well established [22–26] due to the spatial localization of the orbital wave functions. The same approach was applied to the interpretation of $5d$ transition-metal Mott insulators, notably iridates and GaTa₄Se₈, despite the $5d$ orbitals being substantially more extended than their $3d$ counterparts [7,27,28]. Our key finding is that the RIXS spectra from $1T$ -TaS₂ qualitatively deviate from the orbital-multiplet predictions and hence from a localized electron wave-function theory. In contrast, the RIXS excitations can be explained by orbital excitations from an extended electron wave function and, by taking into account the broken symmetry of the crystal field, indicate that polaronic effects dominate the response function of the insulating state at low energies. Our results suggest that the nature of $1T$ -TaS₂ is not a textbook Mott insulator but one close to a band insulator. Moreover, our calculations demonstrate that RIXS and band-theory based calculations can work in concert describing orbital excitations in materials with itinerant electrons.

II. RESULTS

The RIXS measurements were performed at the 27-ID-B (the MERIX endstation) of the Advanced Photon Source with a total energy resolution around 63 meV. The incident x ray was monochromatized at the Ta L_3 edge. A schematic of the RIXS process at the Ta L_3 edge is displayed in Fig. 1(b). The incident x-ray photon excites an electron from the Ta $2p$ core level to the empty $5d$ levels above the Fermi level. Electrons in the Ta $5d$ levels subsequently recombine with the $2p$ core hole and emit an x-ray photon. The energy loss between the incident and the scattered x rays thus contains information about the low-energy electronic excitations in the material. The x-ray absorption spectra from $1T$ -TaS₂ and the reference Ta metal are plotted in Fig. 1(c). In Fig. 1(d) we show the RIXS spectra as a function of the incident energy [marked with vertical black lines in Fig. 1(c)] across the Ta L_3 edge at a base temperature between 10 ~ 15 K. Further details about the x-ray measurements as well as the material synthesis and characterization are presented in the Supplemental Material [29]. To zeroth order, we observe a series of energy-loss features (marked with the red arrows) within the

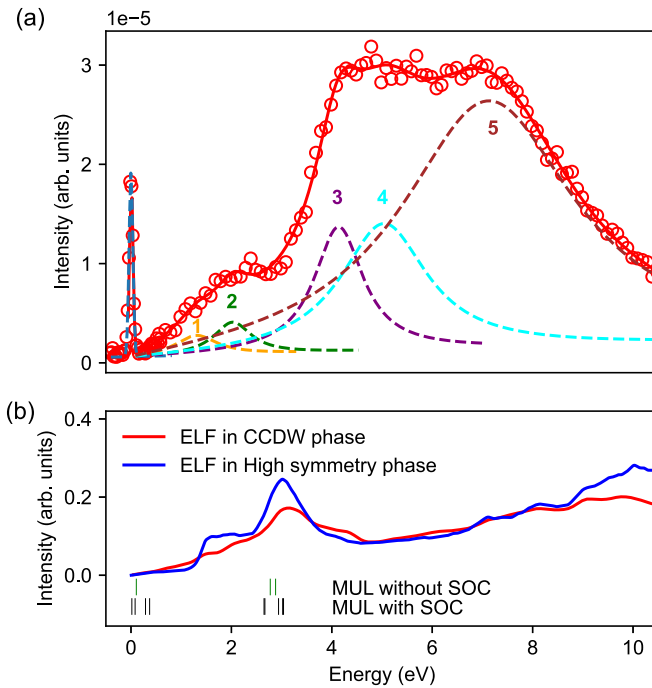


FIG. 2. Comparing measured and calculated energy-loss features. (a) RIXS spectrum at incident energy of 9882 eV. Open red circles are experimental data and solid red line is fit. Individual components of fit corresponding to each energy-loss feature are plotted using dashed lines. (b) Energy-loss function (ELF) in CCDW phase (red) and high-symmetry phase (blue) calculated using DFT. Energies of orbital excitations from multiplet (MUL) calculations with and without SOC are marked using black and green vertical markers, respectively.

first 10 eV, which do not depend on the incident x-ray energy. In comparison, the Ta fluorescence onsets above the Ta L_3 edge, corresponding to the energy-loss features that increase linearly with the incident x-ray energy with a slope of unity. It is apparent that the Ta fluorescence only accounts for a very small fraction of the RIXS spectral weight. This is consistent with other Ta-containing materials, e.g., GaTa_4Se_8 [7], and in contrast to the scenario in itinerant materials where the fluorescence is supposed to dominate the spectral intensity. Notably, the RIXS peaks from the Mott insulator GaTa_4Se_8 were interpreted satisfactorily using the orbital multiplets [7]. Indeed, at first glance, our RIXS measurements seem to suggest that $1T\text{-TaS}_2$ is better described in terms of electrons with strong local correlations as expected in a typical Mott insulator.

We performed a multiple peak fitting to quantify the energy-loss features in $1T\text{-TaS}_2$ and compared them with the multiplet theory predictions. Figure 2(a) displays the RIXS spectra at the incident energy of 9882 eV. This is at the peak of the Ta L_3 edge and where the x-ray Raman peaks are most prominent. As a comparison, in iridates the RIXS features are the strongest at the Ir L_3 pre-edge, 3 eV lower than the absorption peak [6,27,28]. In $1T\text{-TaS}_2$, five energy-loss features are needed to describe the RIXS spectra. We list the position and the full width at half maximum (FWHM) of these peaks in Table I. Each energy-loss peak is described using a

TABLE I. Fitted peak positions and full widths at half maximum (FWHMs) from RIXS spectra.

Peak label	Energy (eV)	FWHM (eV)
1	1.30 ± 0.11	1.02 ± 0.33
2	2.02 ± 0.06	0.91 ± 0.33
3	4.14 ± 0.02	1.18 ± 0.11
4	5.04 ± 0.08	2.10 ± 0.30
5	7.11 ± 0.05	4.21 ± 0.16

Lorentzian while the elastic line takes the shape of a Gaussian. The resulting peak positions and FWHMs do not depend sensitively on the choice of line shapes. Most prominently, there are no clear energy-loss features on the order of the reported Mott gap, which were reported to be generally in the range of 170 ~ 450 meV in a series of spectroscopic measurements including scanning tunneling spectroscopy (STS) and Raman spectroscopy [16,45,46]. This lack of a Mott gap feature was further confirmed in our RIXS data collected using a Montel mirror-based spectrometer with 12 meV energy resolution (see Supplemental Material [29] for details), and was in sharp contrast to previous observations in established Mott insulators with localized electron wave functions [6,7,21]. Note that the x-ray penetration depth at the Ta L edge is $\sim 3 \mu\text{m}$. The RIXS signal is therefore not sensitive to the details of the surface termination or stacking. Thus, the absence of features corresponding to the Mott gap points strongly away from a Mott picture of localized electron wave functions.

From Table I, the four peaks with energy losses less than 6 eV have FWHMs broader than the sub-2 eV peaks but comparable to the peak around 3.5 eV in GaTa_4Se_8 [7]. The peak at 7.11 eV is significantly broader, with a FWHM over 4 eV. All these peaks are substantially broader than those in typical iridates [6,27,28]. This, combined with the lack of a peak at the energy of the Mott gap, indicates that the electrons in $1T\text{-TaS}_2$ are substantially less localized, if at all, than those in established Mott insulators.

Indeed, a more detailed look at the RIXS spectra shows that $1T\text{-TaS}_2$ is not a canonical Mott insulator. A multiplet calculation was performed for a single Ta atom by constructing Wannier orbitals centered on the Ta atom. In the Mott limit, the local electronic correlation dominates with a nominal Ta $5d^1$ configuration. As such, we argue the choice of a single Ta atom would suffice to capture the localized $d-d$ excitations if the system were really in the Mott limit. We further note the multiplet calculation captures the role of the ligand S atoms by taking into account the crystal-field splitting and the deformation of the TaS_6 octahedron. Details of the multiplet calculation are in the Supplemental Material [29]. Within the first few eVs, the energy-loss features mainly arise from the crystal-field splitting between the t_{2g} and e_g orbitals. Taking into account the sizable spin-orbit coupling (SOC) of the Ta atom, the t_{2g} level further splits into $J_{\text{eff}} = 1/2$ and $J_{\text{eff}} = 3/2$ states with an energy difference a fraction of an eV, similar to those observed in iridates [6,27,28].

We show the calculated multiplet peaks without (green) and with (black) a SOC of 0.2 eV using vertical solid markers at the bottom of Fig. 2(b) and summarize the results in

TABLE II. Multiplet calculation results based on a single Ta atom with five d-orbitals.

Energy levels with SOC (eV)	<i>d-d</i> excitations with SOC (eV)	Energy levels without SOC (eV)	<i>d-d</i> excitations without SOC (eV)
1.234	0.017/0.082	1.363 (e_g , twofold)	0.106
1.316	0.289/0.371	1.469 (a_{1g})	2.774
1.605	2.65/2.667		
4.255	2.939/2.956	4.243 (e'_g , twofold)	2.88
4.272	3.021/3.038		

Table II. In both calculations, the obtained orbital multiplets deviated from our measurements, suggesting that the energy scales of local electronic correlations and bandwidth do not suffice to explain the insulating behavior of the CCDW phase. This inconsistency is in accordance with the experimental fact that the high-symmetry phase of 1T-TaS₂ is metallic, and that the insulating state only occurs in the presence of the periodic lattice distortion, in contrast to established Mott insulators.

To understand the role of the periodic lattice distortions in 1T-TaS₂, we turn to a band-theoretical description of the excitations. We performed density-functional theory (DFT) calculations for both the high-symmetry unit cell and the $\sqrt{13} \times \sqrt{13} \times 1$ supercell. We note the full CCDW has a supercell of $\sqrt{13} \times \sqrt{13} \times 3$. Our current selection of the supercell is sufficient to describe the in-plane electronic structure of 1T-TaS₂, though the out-of-plane character remains metallic [15,47,48]. In order to properly describe the Ta *d* orbitals, we took the DFT+*U* [49] approach where we used the generalized gradient approximation [50] for semilocal exchange correlation and a Hubbard *U* parameter for onsite electron interactions within Ta *d* orbitals. An effective Hubbard *U* of 2.27 eV was chosen, as determined previously from the first-principles linear response theory [16,48]. We discuss details of the DFT calculations in the Supplemental Material [29]. The high-symmetry band dispersion is displayed in Fig. 3(a)

and overlaid with the projection to the atomic orbital wave functions. It is apparent that the energy-loss features observed in the experiment from 1.57 to 7.11 eV involve not only the Ta 5*d* orbitals, but also possibly Ta 5*p* and the S 3*p* ligand states.

Using the linear response time-dependent DFT [51], we compare the RIXS spectra with the energy-loss function (ELF) calculated as the inverse of the dynamical dielectric function ϵ within the random phase approximation:

$$S(\mathbf{q}, \omega) = -\text{Im}(\epsilon^{-1}),$$

where

$$\epsilon(\bar{q}, \omega) = 1 - V_q \sum_k \frac{f_{k-q} - f_k}{\hbar(\omega + i\delta) + E_{k-q} - E_k}.$$

Details of the calculations are presented in the Supplemental Material [29]. Notably, we did not take into account the effect of the core hole in our calculation as compared to other itinerant-electron based RIXS calculations [52–54], due to computational challenges associated with the size of the supercell. Following Ref. [52], we assume the core hole mainly acts as a scaling factor at resonance, which undoubtedly changes the relative spectral weight of the calculated peaks but is not expected to dramatically alter the position of these peaks. Therefore, we expect that our approach allows us to quantify the delocalized origin of the RIXS spectra and to

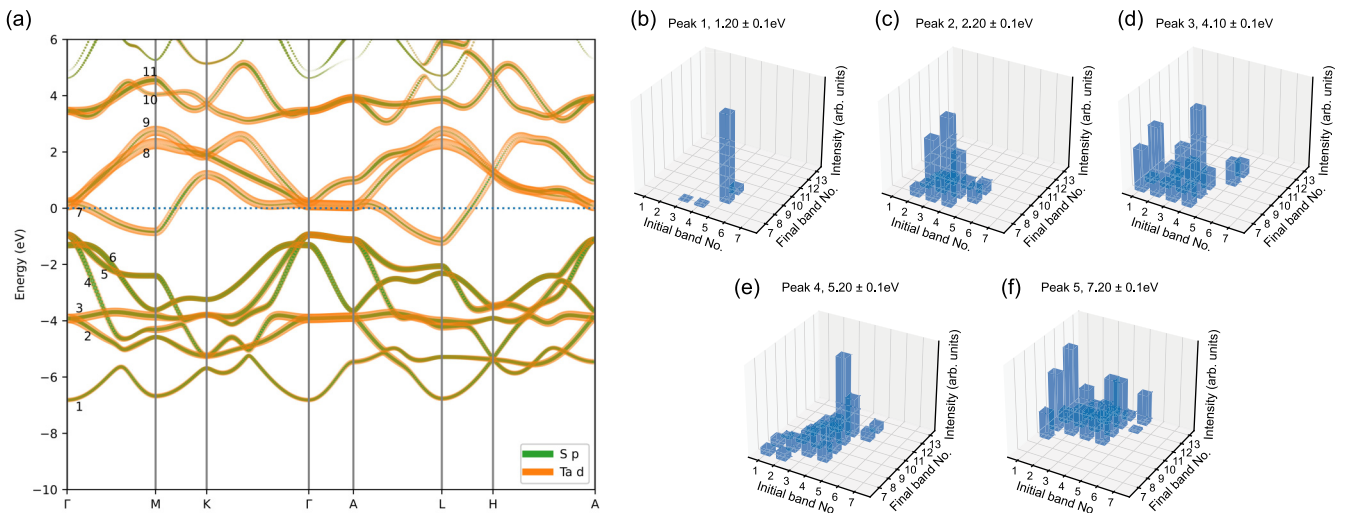


FIG. 3. Band structure in high-symmetry unit cell and band-decomposed contribution to RIXS energy-loss features. (a) Band structure of high-symmetry phase of 1T-TaS₂ overlaid with projection to atomic orbital wave functions. (b)–(f) Calculated interband transition intensities as function of initial and final band numbers at energies of all five excitations observed in RIXS measurement. Energy window is chosen to be ± 0.1 eV for all energy-loss features.

disentangle the role of electronic states near the Fermi level from those of the core levels.

In Fig. 2(b), we show the calculated ELFs at momentum transfer $\mathbf{q} = (-0.1, 0, 0)$ for the high-symmetry and CCDW phases of 1T-TaS₂. The corresponding Brillouin zone (BZ) is defined from the high-symmetry unit cell for both phases. This corresponds to the total momentum transfer $\mathbf{Q} = (-1.1, 0, 6)$ where the RIXS data in Figs. 1 and 2(a) were taken. Here, $\mathbf{Q} = \mathbf{q} + \mathbf{G}$ with \mathbf{G} of reciprocal lattice vector. We chose this \mathbf{Q} position as it is slightly away from the $(-1, 0, 6)$ Bragg peak while keeping the RIXS spectrometer 90° relative to the incident x ray to minimize the elastic peak intensity, following standard RIXS measurement protocols in the hard x-ray regime. Under the independent-particle approximation, a peak in the loss function is associated with a large number of electron-hole transition resonances (i.e., a large density of final states) sharing the same momentum transfer and energy difference. Calculated loss function away from the peaks comes from other electron-hole channels, albeit with smaller total transition probability than at the peak. Due to the itinerant nature of the electrons in this band-based approach, the calculated peaks on the energy-loss function are generally broad, consistent with the observations in Table I. As shown in Fig. 2(b), both high-symmetry and CCDW phases have a prominent feature in their loss function between 2 ~ 3 eV. This increase in the loss function is associated with a zero in the real part of the dielectric function (i.e., a plasmon) (Fig. S5 in the Supplemental Material [29]). In contrast, features at energies <1.5 eV appeared broader in the calculated loss function: these features are the result of an increase in the imaginary part associated with the interband transitions, with significant damping coming from the tail of the Drude peak. Hence, our calculations show that both interband and plasmonic excitations impact the loss function in 1T-TaS₂, and that the interband excitations dominate the low-energy response and are strongly impacted by the structural distortion.

To clarify the detailed orbital nature of the energy-loss features, we further decompose the contribution from relevant bands and atomic orbitals (Ta 5*d* and S 3*p*) to the calculated band structures [Figs. 3(b)–3(f)] by computing the transition intensities as the function of band index of all these excitations. This analysis, performed here for the high-symmetry phase, allows us to assign orbital transitions to the observed RIXS features. The lowest energy-loss feature around 1 eV is almost exclusively composed of the partially filled and the empty bands near the Fermi level, mainly within the partially filled Ta 5*d* state, and is, logically, significantly impacted by the CCDW. The feature at 2 eV corresponds to the transitions from mixed S 3*p* states to Ta 5*d* orbitals, which also make up the energy-loss features at ~ 4, ~ 5, and ~ 7 eV features. Hence, the manifold involved in the RIXS spectrum includes both Ta 5*d* orbitals and S 3*p* orbitals, significantly departing from the pure *d-d* excitations observed in RIXS spectra in some 3*d* transition-metal systems [21,23,24].

The assignment of orbital characters is consistent with the electron density of states measured from STS [16]. Specifically, the STS resolved two sets of electronic states within ±0.5 eV of the Fermi level-localized electrons within ±0.2 eV that constitute the lower and upper Hubbard bands assuming a

Mott insulator perspective, and the more extended electronics states ±0.5 eV and up. Both sets of states are centered around the Ta atom at the center of the CDW but show significant delocalization over the Ta clusters [48], resulting in smaller effective electronic interactions. Importantly, these electronic states contribute to the RIXS spectrum qualitatively different from the 3*d* states in traditional Mott insulators and suggest that explanations of the RIXS spectra from the localized electron wave functions must involve the significant delocalization around the center of distortion.

Interestingly, the S ligand states are at least partially responsible for four of the five energy-loss features, which was little discussed in previous literature. The participation of ligand states is known to be vital in other quantum materials, e.g., cuprates, and most recently nickelates [25,55]. Our result highlights the significance of ligand atoms in yet another quantum material and will affect the interpretations of the orbital textures in 1T-TaS₂ and other dichalcogenides [16,56–58].

III. DISCUSSION

We explore the temperature and momentum dependences of the orbital excitations in further details. In Figure 4(a), we show the temperature dependence of the RIXS spectra at $\mathbf{Q} = (-26/18, -1/9, 6)$, which is a momentum transfer between *M* and *K*, across the CCDW-NCDW transition. This phase transition is of first order with over one order of magnitude change in resistivity. RIXS spectra were collected over both the warming and cooling cycles. We observed no appreciable changes through the phase transition. Note the charge orders in the CCDW and NCDW phases are very similar. Indeed, the NCDW phase is often interpreted as the CCDW domains separated by metallic states in some literatures [59]. In this sense, we do not expect a major change in the electron density of states and the orbital texture over the eV energy scale, except very near the Fermi level [48]. Thus, the persistence of the RIXS spectra can be naturally explained within the band-based framework.

Figure 4(b) shows the RIXS spectra at base temperature of the cryostat along the high-symmetry directions [$\Gamma - M - K - \Gamma - A$, defined in the inset of Fig. 4(c)] of reciprocal space, within the first 4 eV of energy loss. Using the same multiple peak fitting outlined previously, we analyzed the two lowest energy-loss features and plot their dispersions in Fig. 4(c). Most prominent is a pronounced softening of the lowest energy-loss feature from 1.3 eV to below 1 eV, over an extended region in the reciprocal space around Γ and along $\Gamma - A$. In comparison, the second energy-loss feature is generally flat over much of the BZ, apart from two \mathbf{q} points near but not at the *M* point.

The observed softening of the lowest energy-loss feature is unexpected. In the majority of the existing RIXS literature, orbital and charge-transfer excitations over a few eV generally do not depend on the momentum transfer, especially in Mott insulators. Of the few notable exceptions, the Ruddlesden-Popper series of iridates Sr_{*n*+1}Ir_{*n*}O_{3*n*+1} have dispersive orbital excitations between 0.5 and 1 eV from localized spin-orbital moments [5,60]. In Sr₂CuO₃, the quasi-one-dimensional nature of the material gives rise to spin-charge separation and

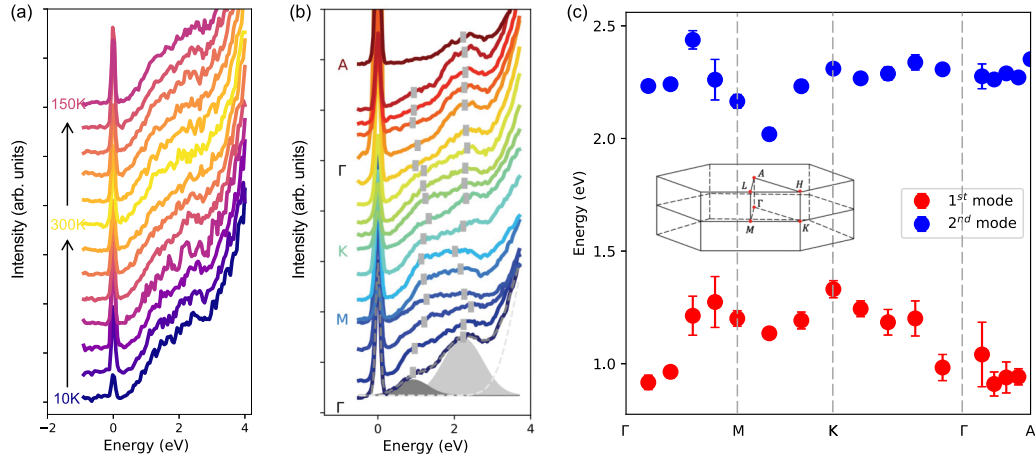


FIG. 4. Temperature and momentum dependences of lowest two orbital excitations. (a) Temperature dependence of RIXS spectra at $(-26/18, -1/9, 6)$ across CCDW-NCDW phase transition, both during warming and cooling cycles. (b) Momentum dependence of RIXS spectra within first 4 eV of energy. Positions of first two energy features from fit are displayed using gray vertical bars. Details of fit at $(-1.1, 0, 6)$ is displayed with contributions from two orbital excitations marked using gray shades. (c) Fitted peak positions of two lowest orbital excitations. Inset: Brillouin zone using high-symmetry unit cell.

leads to several relatively well-defined bosonic modes between 1.5 and 3 eV [61]. In both examples, the electron wave functions are localized. For $1T$ -TaS₂, due to the distortion of the TaS octahedron, there are 13 Ta $5d^1$ electrons per CCDW supercell in plane. Note that the symmetry breaking associated with the interlayer stacking along the c axis is not taken into account in the current calculations due to limited computing power. Given the electron delocalization, this stacking order will lead to further splitting of the electronic bands, which in turn may be responsible for the softening of the ~ 1 eV RIXS feature [13,58].

IV. CONCLUSION

In summary, the orbital excitations in $1T$ -TaS₂ and the absence of excitations corresponding to the assumed Mott gap fundamentally disagree with the accepted scenario of localized electron wave functions. Instead, the orbital excitations can be described qualitatively and semiquantitatively using extended electron wave functions. Our study reveals that the nature of the insulating state of $1T$ -TaS₂ significantly differs from canonical Mott insulators [6,7,21,25–28,62], and underlies the importance of recent theoretical attempts to interpret energy-loss features from a more itinerant picture in similar materials [52,53,63–67]. In these cases, the theoretical prediction required dedicated RIXS measurements either with high-energy resolution challenging at today's instrumentation [63], or over large regions of the reciprocal space that cannot be reached especially for $3d$ elements [64]. The case of $1T$ -TaS₂ shows unambiguously that the low-energy RIXS spectra should incorporate the distortion effect in addition to electronic correlations and will thus affect the understanding and interpretation of future experiments.

ACKNOWLEDGMENTS

The inception of the study, the analysis, and interpretation of the experiment were supported by the U.S. Department of Energy, Office of Science, Basic Energy Sciences, Materials Science and Engineering Division. S.K acknowledges support from the Canada First Research Excellence Fund. The execution of the experiment was supported by Laboratory Directed Research and Development (LDRD) funding from Argonne National Laboratory, provided by the Director, Office of Science, of the U.S. Department of Energy under Contract No. DE-AC02-06CH11357. S.S. and A.H. acknowledge support from the U.S. Department of Energy, Office of Science, Basic Energy Sciences under Award No. DE-SC0018080 and DE-SC0023402. This research used resources of the Advanced Photon Source, a U.S. DOE Office of Science User Facility operated for the DOE Office of Science by Argonne National Laboratory under Contract No. DE-AC02-06CH11357. Work performed at the Center for Nanoscale Materials, a U.S. DOE Office of Science User Facility, was supported by the U.S. DOE, Office of Basic Energy Sciences, under Contract No. DE-AC02-06CH11357. Y.W. was supported by USTC Research Funds of the Double First-Class Initiative (Grant No. YD9990002005). Y.L., W.L., X.L., and Y.-P.S. acknowledge the support from the National Key Research and Development Program under Contract No. 2022YFA1403203, the National Nature Science Foundation of China under Contracts No. 11674326, No. 11874357, and No. 12174365, the Joint Funds of the National Natural Science Foundation of China, and the Chinese Academy of Sciences' Large-Scale Scientific Facility under Contracts No. U1832141, No. U1932217, and No. U2032215. This work was supported by Systematic Fundamental Research Program Leveraging Major Scientific and Technological Infrastructure, Chinese Academy of Sciences under Contract No. JZHKYPT-2021-08.

- [1] J. H. de Boer and E. J. W. Verwey, Semi-conductors with partially and with completely filled 3d-lattice bands, *Proc. Phys. Soc.* **49**, 59 (1937).
- [2] P. A. Lee, N. Nagaosa, and X. G. Wen, Doping a Mott insulator: Physics of high-temperature superconductivity, *Rev. Mod. Phys.* **78**, 17 (2006).
- [3] B. J. Kim, Hosub Jin, S. J. Moon, J.-Y. Kim, B.-G. Park, C. S. Leem, Jaejun Yu, T. W. Noh, C. Kim, S.-J. Oh *et al.*, Novel $J_{\text{eff}} = 1/2$ Mott state induced by relativistic spin-orbit coupling in Sr_2IrO_4 , *Phys. Rev. Lett.* **101**, 076402 (2008).
- [4] Y. Cao, Q. Wang, J. A. Waugh, T. J. Reber, H. X. Li, X. Q. Zhou, S. Parham, S.-R. Park, N. C. Plumb, E. Rotenberg *et al.*, Hallmarks of the Mott-metal crossover in the hole-doped pseudospin-1/2 Mott insulator Sr_2IrO_4 , *Nat. Commun.* **7**, 11367 (2016).
- [5] R. Arita, J. Kuneš, A. V. Kozhevnikov, A. G. Eguiluz, and M. Imada, Ab initio studies on the interplay between spin-orbit interaction and Coulomb correlation in Sr_2IrO_4 and Ba_2IrO_4 , *Phys. Rev. Lett.* **108**, 086403 (2012).
- [6] J. Kim, D. Casa, M. H. Upton, T. Gog, Y.-J. Kim, J. F. Mitchell, M. van Veenendaal, M. Daghofer, J. van den Brink, G. Khaliullin, and B. J. Kim, Magnetic excitation spectra of Sr_2IrO_4 probed by resonant inelastic X-ray scattering: Establishing links to cuprate superconductors, *Phys. Rev. Lett.* **108**, 177003 (2012).
- [7] M. Y. Jeong, S. H. Chang, B. H. Kim, J.-H. Sim, A. Said, D. Casa, T. Gog, E. Janod, L. Cario, S. Yunoki *et al.*, Direct experimental observation of the molecular $J_{\text{eff}} = 3/2$ ground state in the lacunar spinel GaTa_4Se_8 , *Nat. Commun.* **8**, 782 (2017).
- [8] K. Rossnagel, On the origin of charge-density waves in select layered transition-metal dichalcogenides, *J. Phys.: Condens. Matter* **23**, 213001 (2011).
- [9] B. Sipos, A. F. Kusmartseva, A. Akrap, H. Berger, L. Forró, and E. Tutiš, From Mott state to superconductivity in $1T\text{-TaS}_2$, *Nat. Mater.* **7**, 960 (2008).
- [10] X. M. Chen, A. J. Miller, C. Nugroho, G. A. de la Peña, Y. I. Joe, A. Kogar, J. D. Brock, J. Geck, G. J. MacDougall, S. L. Cooper *et al.*, Influence of Ti doping on the incommensurate charge density wave in $1T\text{-TaS}_2$, *Phys. Rev. B* **91**, 245113 (2015).
- [11] P. Fazekas and E. Tosatti, Charge carrier localization in pure and doped $1T\text{-TaS}_2$, *Physica B+C* **99**, 183 (1980).
- [12] L. Perfetti, T. A. Gloor, F. Mila, H. Berger, and M. Grioni, Unexpected periodicity in the quasi-two-dimensional Mott insulator $1T\text{-TaS}_2$ revealed by angle-resolved photoemission, *Phys. Rev. B* **71**, 153101 (2005).
- [13] Y. D. Wang, W. L. Yao, Z. M. Xin, T. T. Han, Z. G. Wang, L. Chen, C. Cai, Yuan Li, and Y. Zhang, Band insulator to Mott insulator transition in $1T\text{-TaS}_2$, *Nat. Commun.* **11**, 4215 (2020).
- [14] L. G. Ma, C. Ye, Y. Yu, X. F. Lu, X. H. Niu, S. Kim, D. L. Feng, D. Tománek, Young-Woo Son, X. H. Chen *et al.*, A metallic mosaic phase and the origin of Mott-insulating state in $1T\text{-TaS}_2$, *Nat. Commun.* **7**, 10956 (2016).
- [15] S.-H. Lee, J. S. Goh, and D. Cho, Origin of the insulating phase and first-order metal-insulator transition in $1T\text{-TaS}_2$, *Phys. Rev. Lett.* **122**, 106404 (2019).
- [16] S. Qiao, X. Li, N. Wang, W. Ruan, C. Ye, P. Cai, Z. Hao, H. Yao, X. Chen, J. Wu *et al.*, Mottness collapse in $1T\text{-TaS}_{2-x}\text{Se}_x$ transition-metal dichalcogenide: An interplay between localized and itinerant orbitals, *Phys. Rev. X* **7**, 041054 (2017).
- [17] J. Lee, K. H. Jin, and H. W. Yeom, Distinguishing a Mott Insulator from a trivial insulator with atomic adsorbates, *Phys. Rev. Lett.* **126**, 196405 (2021).
- [18] K. T. Law and P. A. Lee, $1T\text{-TaS}_2$ as a quantum spin liquid, *Proc. Natl. Acad. Sci. USA* **114**, 6996 (2017).
- [19] Y. J. Yu, Y. Xu, L. P. He, M. Kratochvilova, Y. Y. Huang, J. M. Ni, L. Wang, S.-W. Cheong, J.-G. Park, and S. Y. Li, Heat transport study of the spin liquid candidate $1T\text{-TaS}_2$, *Phys. Rev. B* **96**, 081111(R) (2017).
- [20] S. Mañas-Valero, B. M. Huddart, T. Lancaster, E. Coronado, and F. L. Pratt, Quantum phases and spin liquid properties of $1T\text{-TaS}_2$, *npj Quantum Mater.* **6**, 69 (2021).
- [21] L. J. P. Ament, M. van Veenendaal, T. P. Devereaux, J. P. Hill, J. van den Brink *et al.*, Resonant inelastic x-ray scattering studies of elementary excitations, *Rev. Mod. Phys.* **83**, 705 (2011).
- [22] I. Josefsson, K. Kunnus, S. Schreck, A. Föhlisch, F. de Groot, P. Wernet, and M. Odelius, Ab initio calculations of x-ray spectra: Atomic multiplet and molecular orbital effects in a multiconfigurational SCF approach to the l-edge spectra of transition metal complexes, *J. Phys. Chem. Lett.* **3**, 3565 (2012).
- [23] F. de Groot and A. Kotani, *Core Level Spectroscopy of Solids* (CRC Press, Boca Raton, FL, 2008).
- [24] Y. L. Wang, G. Fabbris, M. P. M. Dean, and G. Kotliar, EDRIXS: An open source toolkit for simulating spectra of resonant inelastic x-ray scattering, *Comput. Phys. Commun.* **243**, 151 (2019).
- [25] M. P. M. Dean, Insights into the high temperature superconducting cuprates from resonant inelastic X-ray scattering, *J. Magn. Magn. Mater.* **376**, 3 (2015).
- [26] C. Monney, A. Uldry, K. J. Zhou, A. Krzton-Maziopa, E. Pomjakushina, V. N. Strocov, B. Delley, and T. Schmitt, Resonant inelastic x-ray scattering at the Fe L_3 edge of the one-dimensional chalcogenide BaFe_2Se_3 , *Phys. Rev. B* **88**, 165103 (2013).
- [27] Y. Wang, R. Wang, J. Kim, M. H. Upton, D. Casa, T. Gog, G. Cao, G. Kotliar, M. P. M. Dean, and X. Liu, Direct detection of dimer orbitals in $\text{Ba}_5\text{AlIr}_2\text{O}_{11}$, *Phys. Rev. Lett.* **122**, 106401 (2019).
- [28] W.-G. Yin, X. Liu, A. M. Tselik, M. P. M. Dean, M. H. Upton, J. Kim, D. Casa, A. Said, T. Gog, T. F. Qi *et al.*, Ferromagnetic exchange anisotropy from antiferromagnetic superexchange in the mixed $3d\text{-}5d$ transition-metal compound $\text{Sr}_3\text{CuIrO}_6$, *Phys. Rev. Lett.* **111**, 057202 (2013).
- [29] See Supplemental Material at <http://link.aps.org/supplemental/10.1103/PhysRevB.108.205105> for the details of material synthesis, x-ray diffraction, x-ray absorption spectroscopy, RIXS measurement, the multiplet calculations, and DFT-based calculations. The Supplemental Material also contains Refs. [30–44].
- [30] Y. V. Shvyd'ko, J. P. Hill, C. A. Burns, D. S. Coburn, B. Brajuskovic, D. Casa, K. Goetze, T. Gog, R. Khachatryan, J.-H. Kim *et al.*, MERIX—Next generation medium energy resolution inelastic X-ray scattering instrument at the APS, *J. Electron. Spectrosc.* **188**, 140 (2013).
- [31] Y. Cao, D. G. Mazzone, D. Meyers, J. P. Hill, X. Liu, S. Wall, and M. P. M. Dean, Ultrafast dynamics of spin and orbital correlations in quantum materials: An energy-and momentum-resolved perspective, *Philos. Trans. R. Soc. A* **377**, 20170480 (2019).

- [32] G. Kresse and F. Jürgen, Efficient iterative schemes for ab initio total-energy calculations using a plane-wave basis set, *Phys. Rev. B* **54**, 11169 (1996).
- [33] P. E. Blöchl, Projector augmented-wave method, *Phys. Rev. B* **50**, 17953 (1994).
- [34] G. Kresse and J. Daniel, From ultrasoft pseudopotentials to the projector augmented-wave method, *Phys. Rev. B* **59**, 1758 (1999).
- [35] N. Marzari, A. A. Mostofi, J. R. Yates, I. Souza, D. Vanderbilt *et al.*, Maximally localized Wannier functions: Theory and applications, *Rev. Mod. Phys.* **84**, 1419 (2012).
- [36] A. A. Mostofi, J. R. Yates, Y. S. Lee, I. Souza, D. Vanderbilt, and N. Marzari, wannier90: A tool for obtaining maximally-localised Wannier functions, *Comput. Phys. Commun.* **178**, 685 (2008).
- [37] J. J. Mortensen, L. B. Hansen, and K. W. Jacobsen, Real-space grid implementation of the projector augmented wave method, *Phys. Rev. B* **71**, 035109 (2005).
- [38] J. Enkovaara, C. Rostgaard, J. J. Mortensen, J. Chen, M. Duřak, L. Ferrighi, J. Gavnholt, C. Glinsvad, V. Haikola, H. A. Hansen *et al.*, Electronic structure calculations with GPAW: A real-space implementation of the projector augmented-wave method, *J. Phys.: Condens. Matter* **22**, 253202 (2010).
- [39] A. H. Larsen, J. J. Mortensen, J. Blomqvist, I. E. Castelli, R. Christensen, M. Duřak, J. Friis, M. N. Groves, B. Hammer, C. Harguset *et al.*, The atomic simulation environment—a Python library for working with atoms, *J. Phys.: Condens. Matter* **29**, 273002 (2017).
- [40] P. E. Blöchl, J. F. Clemens, and S. Johannes, Projector augmented wave method: Ab initio molecular dynamics with full wave functions, *Bull. Mater. Sci.* **26**, 33 (2003).
- [41] E. B. Tadmor, G. S. Smith, N. Bernstein, and E. Kaxiras, Mixed finite element and atomistic formulation for complex crystals, *Phys. Rev. B* **59**, 235 (1999).
- [42] M. P. A. T. Methfessel and A. T. Paxton, High-precision sampling for Brillouin-zone integration in metals, *Phys. Rev. B* **40**, 3616 (1989).
- [43] D. Pines and D. A. Bohm, collective description of electron interactions: II. Collective vs individual particle aspects of the interactions, *Phys. Rev.* **85**, 338 (1952).
- [44] G. Mahan, in *Many-Particle Physics* (Kluwer, Alphen aan den Rijn, Netherlands, 2000), pp. 612–621.
- [45] L. V. Gasparov, K. G. Brown, A. C. Wint, D. B. Tanner, H. Berger, G. Margaritondo, R. Gaál, and L. Forró, Phonon anomaly at the charge ordering transition in $1T$ -TaS₂, *Phys. Rev. B* **66**, 094301 (2002).
- [46] S. Djurdjić Mijin, A. Baum, J. Bekaert, A. Šolajić, J. Pešić, Y. Liu, Ge He, M. V. Milošević, C. Petrovic, Z. V. Popović *et al.*, Probing charge density wave phases and the Mott transition in $1T$ -TaS₂ by inelastic light scattering, *Phys. Rev. B* **103**, 245133 (2021).
- [47] M. Bovet, S. van Smaalen, H. Berger, R. Gaal, L. Forró, L. Schlapbach, and P. Aebi, Interplane coupling in the quasi-two-dimensional $1T$ -TaS₂, *Phys. Rev. B* **67**, 125105 (2003).
- [48] P. Darancet, A. J. Millis, and C. A. Marianetti, Three-dimensional metallic and two-dimensional insulating behavior in octahedral tantalum dichalcogenides, *Phys. Rev. B* **90**, 045134 (2014).
- [49] A. I. Liechtenstein, V. I. Anisimov, and J. Zaanen, Density-functional theory and strong interactions: Orbital ordering in Mott-Hubbard insulators, *Phys. Rev. B* **52**, R5467(R) (1995).
- [50] J. P. Perdew, K. Burke, and M. Ernzerhof, Generalized gradient approximation made simple, *Phys. Rev. Lett.* **77**, 3865 (1996).
- [51] J. Yan, J. J. Mortensen, K. W. Jacobsen, and K. S. Thygesen, Linear density response function in the projector augmented wave method: Applications to solids, surfaces, and interfaces, *Phys. Rev. B* **83**, 245122 (2011).
- [52] B. Barbiellini, J. N. Hancock, C. Monney, Y. Joly, G. Ghiringhelli, L. Braicovich, and T. Schmitt, Inelastic x-ray scattering from valence electrons near absorption edges of FeTe and TiSe₂, *Phys. Rev. B* **89**, 235138 (2014).
- [53] D. Benjamin, I. Klich, and E. Demler, Single-band model of resonant inelastic x-ray scattering by quasiparticles in high-Tc cuprate superconductors, *Phys. Rev. Lett.* **112**, 247002 (2014).
- [54] K. Gilmore, J. Pellicciari, Y. Huang, J. J. Kas, M. Dantz, V. N. Strocov, S. Kasahara, Y. Matsuda, T. Das, T. Shibauchi, and T. Schmitt, Description of resonant inelastic x-ray scattering in correlated metals, *Phys. Rev. X* **11**, 031013 (2021).
- [55] G. Fabbris, D. Meyers, L. Xu, V. M. Katukuri, L. Hozoi, X. Liu, Z.-Y. Chen, J. Okamoto, T. Schmitt, A. Uldry *et al.*, Doping dependence of collective spin and orbital excitations in the spin-1 quantum antiferromagnet La_{2-x}Sr_xNiO₄ observed by X rays, *Phys. Rev. Lett.* **118**, 156402 (2017).
- [56] D. Pasquier and O. V. Yazyev, Crystal field, ligand field, and interorbital effects in two-dimensional transition metal dichalcogenides across the periodic table, *2D Mater.* **6**, 025015 (2019).
- [57] S. Yi, Z. Zhang, and J.-H. Cho, Coupling of charge, lattice, orbital, and spin degrees of freedom in charge density waves in $1T$ -TaS₂, *Phys. Rev. B* **97**, 041413 (2018).
- [58] T. Ritschel, J. Trinckauf, K. Koepf, B. Büchner, M. v. Zimmermann, H. Berger, Y. I. Joe, P. Abbamonte, and J. Geck, Orbital textures and charge density waves in transition metal dichalcogenides, *Nat. Phys.* **11**, 328 (2015).
- [59] X. L. Wu and C. M. Lieber, Hexagonal domain-like charge density wave phase of TaS₂ determined by scanning tunneling microscopy, *Science* **243**, 1703 (1989).
- [60] D. Meyers, Y. Cao, G. Fabbris, N. J. Robinson, L. Hao, C. Frederick, N. Traynor, J. Yang, J. Q. Lin, M. H. Upton *et al.*, Magnetism in iridate heterostructures leveraged by structural distortions, *Sci. Rep.* **9**, 4263 (2019).
- [61] J. Schlappa, K. Wohlfeld, K. J. Zhou, M. Mourigal, M. W. Haverkort, V. N. Strocov, L. Hozoi, C. Monney, S. Nishimoto, S. Singh *et al.*, Spin-orbital separation in the quasi-one-dimensional Mott insulator Sr₂CuO₃, *Nature (London)* **485**, 82 (2012).
- [62] K. Takubo, Y. Yokoyama, H. Wadati, S. Iwasaki, T. Mizokawa, T. Boyko, R. Sutarto, F. He, K. Hashizume, S. Imaizumi *et al.*, Orbital order and fluctuations in the two-leg ladder materials BaFe₂X₃ (X=S and Se) and CsFe₂Se₃, *Phys. Rev. B* **96**, 115157 (2017).
- [63] S. Kourtis, Bulk spectroscopic measurement of the topological charge of Weyl nodes with resonant x rays, *Phys. Rev. B* **94**, 125132 (2016).
- [64] C. Monney, K. J. Zhou, H. Cercellier, Z. Vydrova, M. G. Garnier, G. Monney, V. N. Strocov, H. Berger, H. Beck, T. Schmitt *et al.*, Mapping of electron-hole excitations in the charge-density-wave system $1T$ -TiSe₂ using resonant inelastic x-ray scattering, *Phys. Rev. Lett.* **109**, 047401 (2012).

- [65] D. Sheets, V. Flynn, Jungho Kim, M. Upton, D. Casa, T. Gog, Z. Fisk, M. Dzero, P. F. S. Rosa, D. G. Mazzone *et al.*, Exploring itinerant states in divalent hexaborides using rare-earth L edge resonant inelastic x-ray scattering, *J. Phys.: Condens. Matter* **32**, 135601 (2020).
- [66] C. Monney, M. Herzog, A. Pulkkinen, Y. Huang, J. Pelliciani, P. Olalde-Velasco, N. Katayama, M. Nohara, H. Takagi, T. Schmitt *et al.*, Mapping the unoccupied state dispersions in Ta₂NiSe₅ with resonant inelastic x-ray scattering, *Phys. Rev. B* **102**, 085148 (2020).
- [67] H. Y. Lu, M. Rossi, J.-h. Kim, H. Yavas, A. Said, A. Nag, M. Garcia-Fernandez, S. Agrestini, K. J. Zhou, C. J. Jia *et al.*, Evolution of the electronic structure in Ta₂NiSe₅ across the structural transition revealed by resonant inelastic x-ray scattering, *Phys. Rev. B* **103**, 235159 (2021).